Available online at www.sciencedirect.com
SCIENCE DIRECT®
Sensors and Actuators A 116 (2004) 232–240
SENSORS AND ACTUATORS A PHYSICAL
www.elsevier.com/locate/sna

Vibration measurement with a micromachined mirror in a very-short external cavity laser

Franck Chollet [a,*], Gopal M. Hegde [b], Zhang Xuming [c], Liu Aiqun [c], Anand Asundi [a]

[a] *Nanyang Technological University, School of MPE, 50 Nanyang Avenue, 639798 Singapore*
[b] *Ngee Ann Polytechnic, ECE Department, Photonics Center, Clementi Road, Singapore*
[c] *Nanyang Technological University, School of EEE, Singapore*

Received 31 May 2003; received in revised form 6 April 2004; accepted 16 April 2004
Available online 1 June 2004

Abstract

We have fabricated, modeled and tested a displacement sensor based on an external cavity laser with a micro-mirror integrated with a positioning actuator. We have developed an improved model for simulating the intensity change in the external cavity laser when the feedback from the external mirror exceed 20% of the feedback from the laser facet. A special surface-micromachined mirror has been developed to obtain a very short external cavity laser ($\approx 10\,\mu m$) that allow removing all coupling optical elements in the external cavity. During testing, we could verify the theoretical prediction and achieve a large relative feedback providing a strong intensity modulation. We observed a good angular tolerance suggesting a good manufacturability of the device. The tested device has a noise floor at $5\,pm/\sqrt{Hz}$ above 500 Hz. This sensor could be used as a high sensitivity acceleration sensor.

Keywords: External-cavity laser; Micromachining; MOEMS; Self-mixing; Interferometer; Laser feedback; Accelerometer; Displacement sensor; Large range

1. Introduction

Optical MEMS or MOEMS are experiencing a large growth fueled by the interest in optical telecommunication and particularly in the all-optical switch. However, the interest of mixing optics with MEMS technology goes beyond that well known aspect. For example, optical detectors have an astounding linear range spanning as much as six orders of magnitude, and in another development, interferometry has been shown to yield one of the most sensitive ways of sensing displacement. These two specific aspects call for exploring the possibility of developing displacement sensors based on an optical principle, that could presumably be very small while showing excellent sensitivity and/or large dynamic range.

However, at first, it may not seem obvious that interferometry is a technique that is suitable for integration with MOEMS technology, because it requires many different micro-optical elements (micro-mirrors, micro-beam-splitter) that are not yet on par with their bulk cousins. Although efforts have been made in trying to build a micro-Mach–Zehnder [1] or Michelson interferometer, we will be following another approach [2] using a principle that leads itself to miniaturization: the self-mixing interferometer [3]. The self-mixing interference occurs inside a laser when light is fed back using a mirror external to the laser cavity. When a laser diode is used as the laser cavity, this interferometer is intrinsically compact and has the advantage to show intrinsic gain when compared to system based on filtered photodetector [4]. Then, two other components only are needed to obtain a functional displacement sensor: a photodetector to record the interferogram and, of course, a moving external mirror. A schematic of this principle is shown in Fig. 1. By using a very short external cavity, we are able to relax greatly the tolerance for the assembly and obtain a device with enhanced manufacturability by avoiding the use of a lens [5]. However, the short cavity will require a novel micro-mirror described in the third part of this paper. In the last part we will test the device to measure vibration amplitude.

But before we embark on these descriptions, we will develop a model for the self-mixing interferometer to help design the active part of the sensor.

* Corresponding author. Tel.: +65-6790-6399; fax: +65-6791-1859.
E-mail addresses: mfachollet@ntu.edu.sg (F. Chollet), hgm@np.edu.sg (G.M. Hegde).

0924-4247/$ – see front matter © 2004 Elsevier B.V. All rights reserved.
doi:10.1016/j.sna.2004.04.023

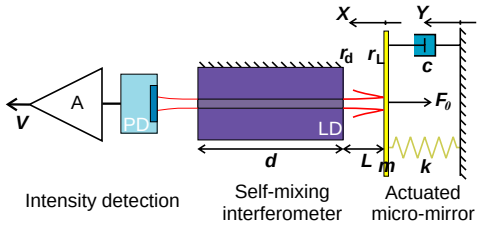

Fig. 1. Schematic of a displacement sensor based on an external cavity laser configuration.

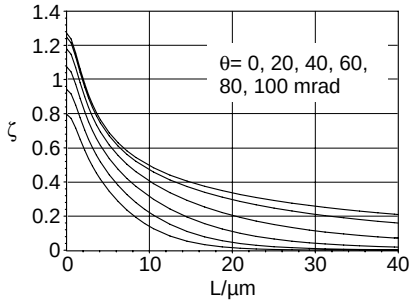

Fig. 2. Evolution of the relative feedback ζ with the external cavity length and the mirror angular misalignment θ ($w_{0x} = 1.9\,\mu m$, $w_{0y} = 0.39\,\mu m$, $\lambda = 0.62\,\mu m$, $r_L = 0.95$, $r_d = 0.34$).

2. Self-mixing interferometer

We develop a steady state model of the feedback in a laser cavity based on the theory derived by Petermann [6], using the stationarity of the field amplitude after one round trip in the cavity.

We have previously established [7] the expression of the change in gain in the cavity due to the feedback as:

$$\Delta g = -\frac{\ln T}{d}, \tag{1}$$

where $T = \sqrt{1+\zeta^2+2\zeta\cos(\tau_L\omega)}$, $\tau_L = 2L/c$ is the time delay in the external cavity and $\omega = \omega_0 + \Delta\omega$. $\Delta\omega$, the shift in wavelength due to the external feedback, is obtained by linearizing the change in gain and the phase shift around ω_0 as:

$$\Delta\omega = T_0^2\alpha \ln T_0 + \arcsin\left[\frac{\zeta\sin(\tau_L\omega_0)}{T_0}\right] \times \frac{1}{\tau_d T_0^2 + \tau_L\zeta[\zeta+\cos(\tau_L\omega_0) - \alpha\sin(\tau_L\omega_0)]}, \tag{2}$$

where $T_0 = T(\omega_0)$, $\alpha = \delta\mu_e'/\delta\mu_e'' \approx 5$, $\tau_d = 2d\bar{\mu}_e'/c$ the time delay in the cavity with a group index of refraction of $\bar{\mu}_e' \approx 3.4$.

In contrary to the previous models [6,8], our equations are established without making the assumption that the relative feedback ($\zeta = f_L/f_d$), ratio between the feedback from the external mirror ($f_L = \gamma r_L(1-r_d^2)$) and the feedback coming from the laser facet ($f_d = r_d$), is small, $\zeta \ll 1$, for example in [6], Chapter 3, Eq. (9.6). Actually, in our configuration this condition is generally not verified [7]. From the expression of the feedback derived in Appendix A and the previous expression, it is possible to plot ζ as a function of the external cavity length and of the mirror angular misalignment (Fig. 2). It is clear that for cavity length of the order of 10 μm, with a moderate angular alignment accuracy, ζ may exceed the value of 0.5, definitely breaking the assumption done in former models.

Still, we are able to simplify our derivation by considering that there are no multiple reflections in the external cavity and that only *the first reflection* is coupled back into the laser. Following previous model [6,8] we may consider that this happens because $r_L \ll 1$, but that is not a very favorable situation because, as we will see later, we want to have a strong relative feedback, thus the reflected wave from the external mirror should be as strong as possible. We show in Appendix A a new reason for neglecting the multiple reflections: in our special configuration it is possible to obtain a strong first reflection—but the subsequent reflections are much dimmed. This happens here because we have a flat mirror without coupling optics: diffraction and angular misalignment assures that the reflections after the first one are coupled back with a very low efficiency.

In order to derive the change in the output power of the LD we will use a linear expression for the power as a function of the polarization current when the current is above the threshold.

$$P = \eta(I_P - I_{th}) + \eta_e I_{th} \tag{3}$$

where P is the output power of the LD, I_P the polarization current, I_{th} the threshold current, η the differential quantum efficiency and η_e the external quantum efficiency. The terms $\eta(I_0 - I_{th})$ and $\eta_e I_{th}$ represents the stimulated and the spontaneous emission, respectively.

Our model assumes that η and η_e are constant and independent of the feedback. Actually, it has been shown that the laser linewidth changes with the feedback [8] and that this assumption is not perfectly true. However, in this work the amount of feedback is never close to the region where appears the so-called 'coherence collapse', as identified by different authors [9].

The change of the laser power due to the feedback is deduced from the modulation of the threshold current.

Actually, the injection current at threshold is proportional to the density of carriers as: [10]

$$\frac{I_{th}}{e} = \frac{tlw\,Bn_p}{\eta_i},$$

where t, w, l are the junction thickness, width and length, respectively, Bn_p is the probability per unit volume that an electron in the conduction band fills a hole in the valence band and η_i the internal quantum efficiency, ratio between the radiative electron/hole recombination and the total number of recombination. For low doped material we have $n =$

$p = n_0$ and thus we can relate a change of threshold current to change of density of carrier as:

$$\Delta I_{\text{th}} = \frac{2twlBn_0e}{\eta_{\text{i}}}\Delta n_{\text{th}}$$

Finally, owing to the linear relationship existing between the gain in the cavity and the density of carriers [6] $g = a(n - n_{\text{t}})$ where n_{t}, the density of carriers at transparency, and a are constants depending on the material, we obtain the shift of threshold current as a function of the change of gain:

$$\Delta I_{\text{th}} = I_{\text{th}} - I_{0th} = b\Delta g \tag{4}$$

where $b \approx 2twlBn_0e/\eta_{\text{i}}a$. The parameters appearing in the expression of b can be obtained from independent measurements and will depend on the material, the structure and the wavelength. From the data found in the literature [6,10] for AlGaAs laser we can estimate $b/twl \approx 3.5\,10^9$ A/m^2.

Thus, when the laser diode is operated at a fixed polarization current I_{P}, the change in threshold current induced by the feedback through a change in internal gain and emitted wavelength, will induce a change in the emitted power, as shown in Fig. 3. It should be noted that this approach still describes a physical model, because the coefficient η and η_e can be obtained from a physical model of the LD [6]. We did not use the more complex expressions for η and η_e to avoid introducing in the model more material properties that have proven to be difficult to measure accurately. In a first order approximation we suppose that these two coefficients are independent of the feedback, and thus could be obtained for each LD used by recording the emitted power as a function of current (P–I characteristic) without feedback. The expression of P as a function of the power without feedback P_0 is then obtained by introducing Eq. (1) into Eq. (4), and expressing the power with feedback using Eq. (3), as:

$$\begin{aligned} P &= P_0\left(1 + \frac{P - P_0}{P_0}\right) \\ &= P_0\left(1 + \frac{-\eta(I_{\text{th}} - I_{0\text{th}}) + \eta_e(I_{\text{th}} - I_{0\text{th}})}{\eta(I_{\text{P}} - I_{0\text{th}}) - \eta_e I_{0\text{th}}}\right) \\ &\approx P_0\left(1 + \frac{(1 - \eta_e/\eta)b/d\ \ln T}{I_{\text{P}} - I_{0\text{th}}}\right) \end{aligned} \tag{5}$$

The dependency of T on L (Eq. (1)) finally links the length of the external cavity with the emitted power. When the decrease in threshold current $(b/d)\ \ln T(\nu)$ exceeds $I_{\text{P}} - I_{0\text{th}}$ the laser stops lasing and we only get spontaneous emission. Using a typical case of a laser operated at 8 mA above the threshold current with a normalized power of 1 without feedback (thus, $\eta = 125$), and taking different values for ζ we have plotted the evolution of the power in Fig. 4 as a function of the cavity length L (we neglect here the spontaneous emission $\eta_e \ll \eta$). We observe a periodic change of intensity with the mirror position, in a way similar to classical interference phenomena. Here, also the period is $\lambda/2$ and suggests that there is little benefit in moving the mirror more than that distance, if we do not want to 'count the fringes'. But the similarity with two-waves interference stops here. We observe for small value of ζ vertically symmetric fringes around the value of power without feedback but when ζ increases above about 0.3, the fringe looses its symmetry, the decrease in power is much larger than the increase.

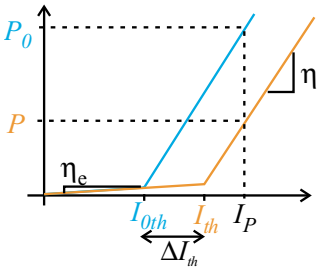

Fig. 3. Linearized model used to derive the change in emitted power induced by the change in threshold current.

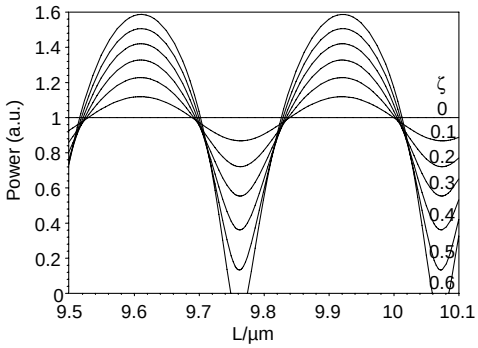

Fig. 4. Power at the laser output versus external cavity length with different relative feedback $\zeta = 0$, 0.1, 0.2, 0.3, 0.4, 0.5, 0.6 (with $c = 3 \times 10^8$ m, $d = 200\,\mu$m, $\mu_e = 3.4$, $\nu_0 = c/0.620 \times 10^{-6}$ Hz, $\alpha = 5$, $b = 2 \times 10^{-6}$ Am, $\eta = 125$).

The sensitivity of the external cavity laser used as a displacement sensor is given by $\mathrm{d}P/\mathrm{d}L$ (the expression is analytic but too long to be shown here), which has been plotted for the same condition of Fig. 4 in Fig. 5. This figure shows a large gain in sensitivity that can be expected by operating the laser with a medium relative feedback ($\zeta > 0.4$). However, we see that the sensitivity is changing quickly with the

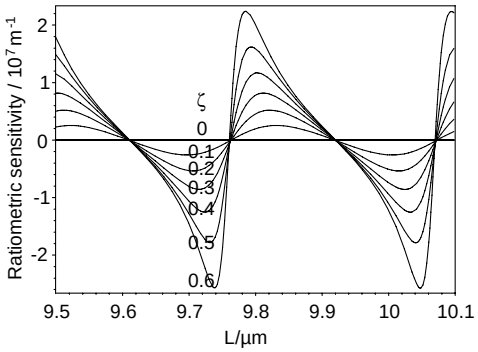

Fig. 5. Ratiometric sensitivity $(1/P_0)\mathrm{d}P/\mathrm{d}L$ Wm^{-1}/W vs. external cavity length with different relative feedback $\zeta = 0$, 0.1, 0.2, 0.3, 0.4, 0.5, 0.6 (same conditions as in Fig. 4).

position, thus to obtain a device that can be used efficiently, an actuator needs to be integrated with the mirror to position it near the peak of sensitivity. Moreover, if we want to use the largest sensitivity, it is clear that we will obtain a small linear range and a scheme based on position feedback (using the integrated actuator) will be needed.

The sensitivity ($\mathrm{W\,m^{-1}}$) depends on the emitted power P_0 of the LD. Thus, to obtain a large signal change we would need large polarization current I_P. However, in this case the spontaneous emission increases, decreasing the maximum visibility of the self-mixing interference fringes and reducing the sensitivity. An optimum can be found and for our arrangement, Fig. 2 revels that we may expect $\zeta > 0.5$ with $L \approx 10\,\mu\mathrm{m}$. Thus, a polarization current of 8 mA above the threshold without feedback as used to plot Fig. 4 is appropriate because the fringe will then have the maximum possible visibility if we take into account the spontaneous emission (not shown in Fig. 4). In this case, the maximum sensitivity is $1.8\,10^7 P_0\,\mathrm{m^{-1}}$, or about 10^5 W/m for a typical 5 mW LD, meaning that if the photodetector can detect intensity change in the order of 0.05 μW (corresponding to a dynamic range of 10^5), we should be able to detect displacement below 1 pm.

The dynamic of the sensor as a displacement sensor is limited by this resolution and also by the maximum displacement that we can measure unambiguously. As observed in Fig. 4, this maximum range is about $\lambda/4 \approx 150$ nm but of course it could be extended if we choose to allow to 'count the fringes'.

The plot of the sensitivity revels that for large ζ the power change is asymmetric, not only vertically, but also along the displacement axis. Actually, it can be seen that the slope along the decreasing part of the curve is larger than along the rising side. This asymmetry increases with the external cavity length and it is a well known—and much more pronounced—feature with long external cavity [8].

When the suspended mirror with its actuator is modeled as a 1-DOF mass-spring-damper lumped system (cf. Fig. 1) we can show that for frequency much below the natural frequency $\omega_\mathrm{n} = \sqrt{k/m}$, the amplitude of the mirror displacement is:

$$Z \approx \frac{A}{\omega_\mathrm{n}^2} + \frac{F_0}{k}, \tag{6}$$

which is proportional to the amplitude of the frame acceleration A. Thus, the suspended mirror may be used in conjunction with the self-mixing interferometer to measure acceleration, and the force developed by the actuator F_0 will allow to bias the position of the mirror to obtain the largest sensitivity.

3. Micromachined external cavity mirror

From the previous discussion the external mirror should have:

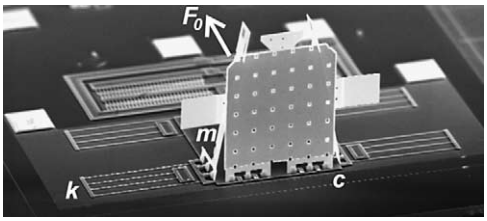

Fig. 6. General view of the assembled 3D-mirror.

- large reflection coefficient to increase the external feedback coefficient f_L;
- unobstructed front surface to come as close as 10 μm with the LD to increase the sensitivity;
- integrated actuator with a range of $\lambda_0/2$ to position the mirror at the maximum of sensitivity.

The mirror has been fabricated using a standard micro-fabrication process, using two structural layers of poly-silicon, a gold coating, one ground plane and two sacrificial layers of SiO_2. Fig. 6 is a general view of the mirror. We can see the integrated actuator, at the rear, and the mirror suspension made of four folded-beam springs.

3.1. A 3D mirror

The structure is patterned in a stack of different layers and then is folded to its 3D shape with micro-probes under a microscope. Our objective to bring the mirror within 10 μm in front of the laser facet has necessitated the development of a new, more compact, type of hinge. In contrast to previously developed hinges [11], the beams used to constrain the axis (i.e., the staple) are cantilevered and attached only on one side of the mirror. A close-up of the designed hinge is shown in Fig. 7. With this special design, the distance between the plane of the mirror and the edge of the supporting structure can be less than 10 μm, allowing to position the laser diode without mechanical interference.

Moreover, we have revisited the mirror locking mechanism to improve its accuracy. Usually 'precision locks' placed on each side of the folded structure [1] are used instead of the initial spring lock [11] that was much more

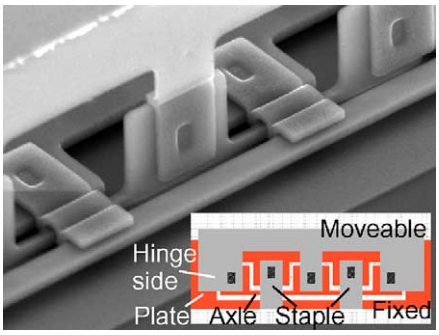

Fig. 7. Close-up on the suspended hinge of the mirror and its typical layout.

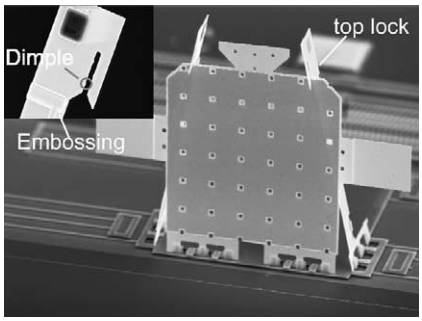

Fig. 8. Close-up on the precision lock on top of the mirror with an enlargement of a locking structure (we can see the embossed shape of the spring in the plate that has a stiffening effect).

clever but not accurate enough for most optical elements positioning. However, we found that the precision locks could be improved if instead of constraining the folded structure at its *side*, at about half the height of the plate, we constrained the *top* of the plate. Obviously, for the same fabrication tolerance and clearance the incertitude angle is divided by two compared to the usual design. Fig. 8 shows a close-up of the engaged lock positioning the folded mirror. Note that they have been designed to not protrude more than 10 μm from the mirror plane. The locking structure has been featured with bumps to define precisely the contact points with the mirror plate leaving a clearance of about 0.5 μm on each side of the mirror plate. Including the clearance at the hinge ≈ 0.75 μm, corresponding to the thickness of the second sacrificial layer, we estimate the maximum error of angle that can be expected with this structure to about $\sin^{-1}((0.75+0.5)/300) \approx 4$ mrad (0.23°).

This small value of the angular error can be easily tolerated by the system as can be seen from Fig. 2, making it possible to align the mirror with the laser diode facet by using only the wafer plane as a reference plane. Thus, we do not need to align the LD directly with respect to the mirror, and a passive alignment strategy can be used, simplifying greatly the packaging procedure.

3.2. A reflecting mirror

As we have seen in Section 2 we need a mirror with a large reflection coefficient to obtain a large relative feedback coefficient and thus the largest sensitivity to displacement. There are different factors that affect significantly the effective reflectance of the mirror: the reflection coefficient of the mirror coating at the laser wavelength, the planarity and the roughness of the surface. Table 1 lists these parameters for different architecture of mirror.

The curvature of the mirror is due to the gradient of stress along its thickness because it is composed of different materials. It is important to maintain it as low as possible because it is related to a local tilt of the mirror that decrease the relative feedback coefficient as we have shown in Fig. 2. The value given in Table 1 is the extreme value at the mirror edge, and in practice it is much lower (<10 mrad) because we use the mirror near its center.

Table 1
Measured radius of curvature and surface roughness of different mirror design with calculated maximum tilt angle, and reflection coefficient at 0.62μm (neglecting multiple reflections)

Mirror	ρ (mm)	Max. tilt (mrad)	R_{RMS} (Å)	r_L
3.5 μm Poly + 0.5 μm Ti/Au	22	7	23	0.97
1.5 μm Poly + 0.5 μm Ti/Au	1.9	80	26	0.97
2.0 μm Poly	∞	<1	35	0.57
1.5 μm Poly	∞	<1	32	0.57

It may be thought to use this stress-induced curvature in order to obtain a cheap converging mirror, however, the difficulty to control stress in the deposited layer (the metal is under a tensile stress varying between 0 and 40 MPa and the poly-Si under a compressive stress in a 0–20 MPa range ...) makes it an unpractical solution.

The roughness of the surface is very low (we have $R_{RMS} < \lambda_0/200$ and $R_t < \lambda_0/50$) and the reflection coefficient is not affected significantly by this figure. It is an interesting feature of the folded micro-mirror compared to an etched mirror. In our case, the surface of the mirror is controlled by the conformal deposition of layer onto an atomically flat substrate and not by an etching mechanism, which generally yields a rougher surface [12].

3.3. An actuated mirror

Section 2 has shown that a range of about $\lambda_0/2$ is required for the actuator to position the mirror where the sensitivity is the highest.

For a comb-drive actuator [13], the relationship between voltage and displacement is given by:

$$x = aV^2,$$

where the deflection constant $a = N\varepsilon_0 h/gk$. Here, N is the number of finger, h the thickness of the electrodes, g the distance between the electrodes and k the suspension spring constant. From simple beam theory [14], it is possible to obtain $k = 8Ehw^3/(L_1^3 + L_2^3)$, relating the spring constant to the physical dimension of the four springs of the suspension (h is the beam thickness, w the beams width and L_1 and L_2 the length of the two parts of the folded beams) and to the material Young's modulus ($E = 170$ GPa).

We measured the dc characteristics of the mirror/actuator with a system based on an optical microscope with a resolution of about ±0.15 μm. From the fit of the experimental curve, the 156-fingers actuator has an actuation constant $a = 3.98\ \text{nm/V}^2$. Our design can thus ensure that the required 0.35 μm ($\approx \lambda_0/2$) displacement of the mirror is obtained with a voltage of less than 10 V, compatible with standard CMOS circuitry.

A preliminary estimation of the fabrication process uniformity on 7 wafers revealed that the designed 2 μm wide

Table 2
Modeled characteristics of the actuator (the mass of the mirror used in the analytical model is 1.95 μg as given from geometry and material density)

Beam width (μm)	Experimental		Analytical			IntelliSuite™		
	ω_0 (rad/s)	Q	k (N m)	a (nm/V^2)	ω_n (rad/s)	k (N m)	a (nm/V^2)	ω_n (rad/s)
2.0	17090	4.8	0.58	2.37	17246	0.59	3.98	17151
1.75	13820	4.5	0.38	3.22	13959	0.39	5.40	13880

beams have actual width varying between 2 and 1.75 μm. The action of this narrowing of the beam is two-fold: it decreases the spring constant of the suspension but on the other hand it decreases the electrostatic force of the actuator by enlarging the gap. We studied in more detail the dynamic of two mirrors fabricated on two different wafers and representing these two extreme cases. Table 2 summarizes these experimental results together with the simulation results using simple analytical formula based on Rayleigh's analysis and using IntelliSuite™. We may note that if the finite element analysis is superfluous for estimating the purely mechanical characteristics (k, ω_n), the analysis of the electrostatic force using analytical formulation suffers from a systematic underestimation. This can be traced to the neglected 3D fields in the analytical model that are important for this structure where the gap to thickness ratio is large. The natural frequency values match the experiment very well and the deflection constant a for a beam width of 2 μm agrees with the experimental value obtained above, validating the numerical model.

Still, the damping has proven to be more difficult to estimate and the analytical and numerical model could only gives results with large error. The reason seems to lie in the difficulty to model some of the sources of damping existing in the structure, like the air damping between the comb fingers. Actually, this source of damping seems to be an important part of the total damping almost as important as the Couette's flow damping arising below the horizontal plate. In the other hand, air drag seems to be negligible, because the change in the Q factor when the mirror was assembled vertically and when it was folded was in the margin of error of the experiment.

4. Experiment and discussion

The Fabry–Perot laser diode used is a Sanyo HL6720G index guided with a double hetero structure emitting at 670 nm. Its threshold current has been found to be around 35 mA and we generally operated it around 43 mA where it delivers a power of several milliWatts. The photo-detector used is the silicon PIN diode integrated near the rear facet of the laser diode whose signal is amplified by a low-noise battery operated amplifier and directed to an oscilloscope or a spectrum analyzer. To help the testing by removing the uncertainty linked with the integrated actuator we have mounted the mirror on a piezoelectric actuator with a 'thumbtack' holder. This arrangement allows to reach very near the packaged diode laser without being hampered by the casing and the sub-mount of the diode. The piezoelectric actuator has been separately calibrated with a custom-made Michelson interferometer, and we found a sensitivity of about 100 nm/V. The tip of the thumbtack has been coated with a black absorbing layer prior to the attachment of the micromachined gold mirror, to avoid spurious reflection. The assembly is observed through a stereo-microscope to position precisely the mirror near the external facet of the laser. A schematic of the testing set-up is shown in Fig. 9. Before taking any measurements the laser diode is left on during several minutes so that its temperature is stabilized. The mirror is moved periodically with the piezo-actuator and we record the driving signal for the actuator and the power measured by the photodetector as shown in Fig. 10.

The power fluctuation is higly non-linear and has a period of about 330 nm, which is half the wavelength of the laser, as predicted by the theory. The response (a) and (b) are obtained for two different external cavity length. With the shorter external cavity we were able to increase the feedback ratio ζ and obtain non-symmetric fluctuation with a very large visibility of the fringe, favorable for the use of the system as a displacement sensor. By estimating the alignment accuracy at about 1.5°(≈ 30 mrad), we obtain from the theoretical curve of Fig. 2 that for the 25 μm cavity length (case a) ζ is about 0.2, while for the cavity of 10 μm (case b) it is slightly below 0.5. By comparing the theoretical curve of Fig. 4 for these two values with the experimental curves, it can be seen that the agreement is very good, validating the model and suggesting that it can be used for the design of such structure.

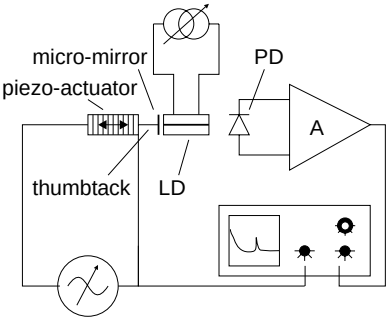

Fig. 9. Schematic of the set-up used for testing the displacement sensor.

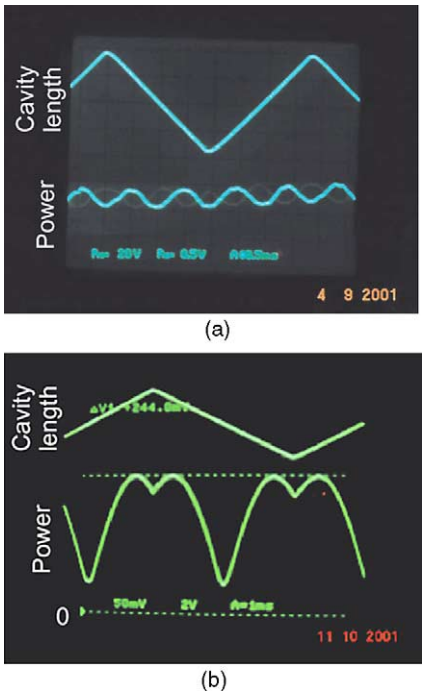

Fig. 10. Oscillogram of the emitted power and the voltage applied to the piezo-actuator (triangular trace) with an external cavity length about: (a) 25 μm and (b) 10 μm.

Part of the discrepancy with the model originates from the hypothesis that the power emitted (and measured by the PIN photodiode) is proportional to the intensity. Actually, this depends on the profile of the laser emission and is not strictly true.

By using a spectrum analyzer, we were able to measure the noise existing in the system as a function of the current of polarization in the diode (Fig. 11). As changing the polarization current can also change the sensitivity, we took the precaution to use the same optical sensitivity by changing slightly the cavity length until we obtain roughly the same output for a constant reference displacement at 1350 Hz. During that time the gain of the photodetection circuit was not changed. It is observed here that the noise level increases with the polarization current. Actually, by increasing the polarization current we increase the emitted power and thus increase the noise due to the fluctuation in the threshold current. However, as we noted above, at the same time we increase the sensitivity until the contrast of the interference fringes drops (in this case above 41 mA), making it interesting to work with large enough polarization current. The signal spectrum shows that above 200 Hz the noise increases with the LD polarization current and is thus linked with the laser diode. This implies that above 200 Hz, the photodiode noise and the amplifier noise are not the limiting factor for the sensor resolution and this range of frequency can be used to estimate the resolution of the system with the LD used. Below 200 Hz the noise is not affected by the polarization current, and is thus presumably linked with elements outside the LD cavity. The photodetector $1/f$ noise is certainly what explains the noise profile below 30 Hz. However, the large bump around 80 Hz is apparently due to mechanical resonance of the mirror testing assembly. Actually, the amplitude of this signal does not change with the LD polarization current, whereas it did vary with the sensitivity, pinpointing its origin in the mechanical/vibration signal. As a further proof of its presence in the measurand, this noise can even be seen as sidelobes on the signal at 1350 Hz.

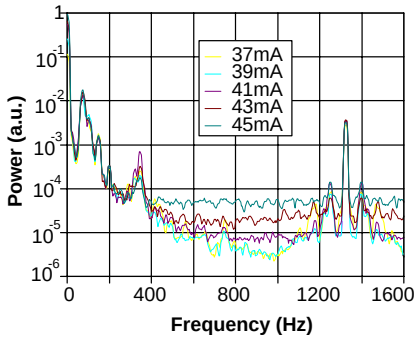

Fig. 11. Measured noise spectrum as a function of the polarization current I_0 for a 15 μm long cavity.

Owing to the existence of the mechanical low-frequency noise, the resolution of the sensor could not be established using low-frequency signal and a broad-band detector. Thus, we used the spectrum analyzer and measured simultaneously the sensor noise and signal. The external cavity length was about 10 μm and the LD polarization current was set at 43 mA. Then we adjusted slightly the cavity length to obtain the largest sensitivity, and vibrated the mirror at 2 kHz (well above the 200 Hz limit and away from the resonance of the piezo-actuator) with an amplitude of 0.2 nm (the smallest displacement reliably obtained with the piezo-actuator). The signal recorded in a band of 16 Hz was more than 10 dB above the noise floor. From this measurement the resolution of the sensor can be estimated as $5\,\text{pm}/\sqrt{\text{Hz}}$. This value compares favorably with the predicted value of 1 pm, the discrepancy being attributed to the coarseness of the noise model in our analysis. This resolution would allow to obtain an accelerometer with a resolution in the order of $1\,\mu\text{g}/\sqrt{\text{Hz}}$ with a slightly softer mirror suspension.

5. Conclusion

We have studied a self-mixing interferometer using a micro-machined mirror with a very short external cavity configuration. Contrary to previous models, the model of the external cavity laser that we have developed is still valid when the relative feedback is larger than 0.2. Combining it with a Gaussian analysis of the reflected field, we were able to propose a new argument for neglecting the reflection in the external cavity. Moreover, the model allowed taking into account the mirror angular misalignment and thus relate accurately the physical characteristics of the device to

its behavior, something not attained by previous authors. We have shown that, in our configuration, an angular misalignment of 20–40 mrad would decrease the noise in the system through the suppression of the multiple reflections in the external cavity while still maintaining a large feedback.

We developed a surface-micromachined mirror that we integrated with a micro-actuator, a fundamental progress to achieve simple assembly of such system. The mirror has compact hinges and a new top-locking mechanism that keep the mirror perpendicular to the substrate with minimum angular error, again simplifying the sensor assembly. The test reveled that without coupling lenses we were still able to reach a regime of medium coupling ($\zeta > 0.4$), where the interference fringes have a large visibility, and obtain a sensor with high sensitivity. The system has then been tested as a vibration sensor, and the resolution achieved around 2 kHz is 5 pm/$\sqrt{\text{Hz}}$.

Although the noise at low frequency has so far prevented us to use the device as a broad-band acceleration sensor, we are developing a rugged integrated package to suppress the noise of mechanical origin. We are also studying the possibility to modulate the position of the mirror with the integrated actuator to use heterodyne detection to measure acceleration at low frequency. The very high displacement sensitivity of the sensor is very promising for acceleration sensing and simple calculation shows that resolution of 1 μg/$\sqrt{\text{Hz}}$ can be achieved.

Acknowledgements

We want to thanks Mr. Andrew Sabaratnam manager of the Photonics Centre in Ngee Ann Polytechnic for his encouragement, and Mr. S.S. Yong for the help provided during testing.

Appendix A

Our model of the external cavity laser is based on the assumption that we can neglect the multiple reflections arising in the external cavity while still having a large feedback coefficient for the external mirror. To show that this seemingly contradictory condition is verified with our configuration, we will study the coupling of light back into the laser diode after reflection on the mirror. We use a model based on a elliptic Gaussian approximation of the modal field and the reflected field. The optical field expression includes terms describing a tilt and an offset in addition to the diffraction (i.e. beam spreading) for studying the effect of an angular misalignment of the mirror:

$$E(x, y, s, \theta_x, \theta_y) = \sqrt{\frac{2P_0}{w_x w_y \pi}}\, \mathrm{e}^{\mathrm{i}(k/2)(2\theta_x x + 2\theta_y y + x^2/R_x + y^2/R_y)}\, \mathrm{e}^{-(x^2/w_x^2 + y^2/w_y^2)}$$

where P_0 is the power carried by the beam (i.e., $P_0 = \iint E_0 E_0^* \,\mathrm{d}x\,\mathrm{d}y$), $w_x = w_{0x}\sqrt{(1 + (\lambda s/(\pi w_{0x}^2))^2)}$ is the beam waist at s, $R_x = s(1 + (\pi w_{0x}^2/(\lambda s))^2)$ is the Gaussian field curvature at s, θ_x is the phase front tilt for the X-axis (with similar terms along the Y-axis) and s the propagation distance of the beam. Note that we use a non-astigmatic description of the elliptic field, because the LD is index guided.

Then the amplitude coupling efficiency is estimated by computing the modulus of the overlap integral between the reflected field and the mode field, as:

$$\gamma(s, \theta_x, \theta_y, \delta_x, \delta_y) = \left| \int_{-\infty}^{+\infty} \int_{-\infty}^{+\infty} E(x, y, s, \theta_x, \theta_y) E_0(x - \delta_x, y - \delta_y)\,\mathrm{d}x\,\mathrm{d}y \right|$$

where E_0 is the mode field (i.e. $\theta_x = \theta_y = 0$ and $s = 0$, that is $w_x^y = w_{0x}^{0y}$ and $R_x^y = \infty$) and where δ_x and δ_y represent an offset between the reflected beam and the mode field.

This integral has an analytical solution, but too complex to be given here in the general case. When there is no tilt nor offset the expression of the amplitude coupling coefficient for an elliptical beam is:

$$\gamma(s) = 2\pi w_{0x} w_{0y} \sqrt[4]{\frac{\pi^2 w_{0x}^4 + \lambda^2 s^2}{\lambda^4 s^4 + 5\pi^2 w_{0x}^4 \lambda^2 s^2 + 4\pi^4 w_{0x}^8}} \times \sqrt[4]{\frac{\pi^2 w_{0y}^4 + \lambda^2 s^2}{\lambda^4 s^4 + 5\pi^2 w_{0y}^4 \lambda^2 s^2 + 4\pi^4 w_{0y}^8}}$$

When $w_{0x} = w_{0y} = w_0$ (cylindrical beam) this expression is the same as previous results found in the literature for optical fiber coupling [15,16]. We should note here that we neglect a small phase term in the amplitude coupling coefficient that changes only slightly the phase delay induced by the propagation ($2\pi 2L/\lambda_0$), which is already taken into account in the model.

The expression for γ is valid also when the beam experiences multiple reflections on the mirror and on the laser facet. The feedback coefficient for the nth reflection can thus be expressed as:

$$f_L^n = \gamma_n r_L^n r_\mathrm{d}^{n-1}(1 - r_\mathrm{d}^2),$$

where n is the rank of the reflection. In the case of an external mirror tilted by an angle θ with respect to the X-axis only, the external feedback coefficient for the nth reflection becomes $\gamma_n = \gamma(2nL, 2n\theta, 0, -2n^2\theta L, 0)$ as can be obtained by using simple geometry and the diagram of Fig. 12. Thus, we can plot the variation of f_L as a function of the external cavity length for the first and subsequent reflections, and for different value of the tilt angle, as shown in Fig. 13. It appears clearly that the feedback from the second and third reflection is much weaker than from the first reflection, especially when the mirror has a small tilt. This result justify

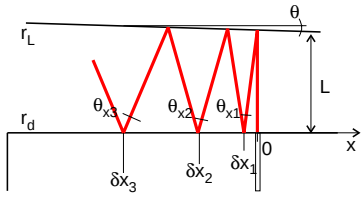

Fig. 12. Schematic view of the beam multiple reflections in the external cavity with a tilted mirror.

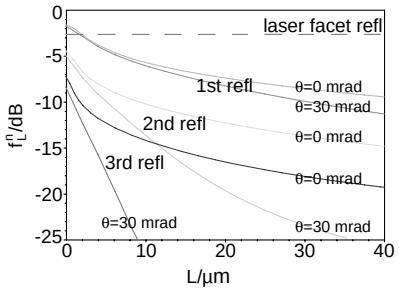

Fig. 13. Feedback coefficient for the first second and third reflection as a function of the external cavity length with a perfectly aligned mirror ($\theta = 0$) and with a mirror tilted by 30 mrad (1.7°). The dashed line shows the feedback coefficient from the laser facet ($w_{0x} = 1.9\,\mu m$, $w_{0y} = 0.39\,\mu m$, $\lambda = 0.62\,\mu m$, $r_L = 0.95$, $r_d = 0.54$).

the hypothesis done in the derivation of the model for the system.

Moreover, when we compare the curve for the first reflection with and without tilt, it is also clear that the feedback coefficient is not too sensitive to the tilt of the mirror. It means that a small tilt is tolerable, which would simplify greatly the assembly/alignment procedure. Moreover, it shows that introducing a small tilt angle is an effective way to suppress the multiple reflections, and the associated noise, while keeping a large feedback from the external cavity. This are the main advantages of using a very-short external cavity, as opposed to a standard set-up with longer cavity and coupling optics.

References

[1] L. Lin, S. Lee, K. Pister, M. Wu, Micro-machined three-dimensional micro-optics for integrated free-space optical system, IEEE Photon. Technol. Lett. 6 (1994) 1445–1447.
[2] R. Miles, A. Dandridge, A. Tveten, T. Giallorenzi, An external cavity diode laser sensor, J. Lightwave Technol. 1 (1983) 81–93.
[3] Y. Sidorin, M. Blomberg, P. Karioja, Demonstration of a tunable hybrid laser diode using an electrostatically tunable silicon micromachined Fabry–Perot interferometer device, IEEE Photon. Technol. Lett. 11 (1999) 18–20.
[4] R.L. Waters, M.E. Aklufi, Micromachined Fabry–Perot interferometer for motion detection, Appl. Phys. Lett. 81 (2002) 3320–3322.
[5] J. Shimada, Y. Kotagiri, O. Ohguchi, R. Sawada, Optical micro displacement sensor using a composite cavity laser diode integrated with a microlens, J. Micromech. Microeng. 4 (1994) 140–146.
[6] K. Petermann, Laser Diode Modulation and Noise, Kluwer, 1988, Chapter 9, pp. 250–290.
[7] X. Zhang, A. Liu, V. Murukeshan, F. Chollet, Integrated micromachined tunable lasers for all optical network (AON) applications, Sens. Actuators A 97–98 (2002) 54–60.
[8] W.M. Wang, K.T. Grattan, A.W. Palmer, W.J. Boyle, Self-mixing intereference inside a single-mode diode laser for optical sensing applications, J. Lightwave Technol. 12 (1994) 1577–1587.
[9] D. Lenstra, B.H. Verbeeck, A.J. den Boef, Coherence collapse in single-mode semiconductor lasers due to optical feedback, IEEE J. Quantum Electron. 21 (1985) 674–679.
[10] M.J. Adams, A.G. Steventon, W. Devlin, I.D. Henning, Semiconductor Lasers for Long-wavelength Optical-fibre Communications Systems, Peter Peregrinus, 1987, Chapter 3, pp. 19–44.
[11] K. Pister, M. Judy, S. Burgett, R. Fearing, Microfabricated hinges, Sens. Actuators A 33 (1992) 249–256.
[12] C. Marxer, C. Thio, M.-A. Grétillat, N. d Rooij, R. Bättig, O. Anthamatten, B. Valk, P. Vogel, Vertical mirrors fabricated by deep reactive ion etching for fiber-optic switching applications, J. Microelectromech. Syst. 6 (1997) 277–285.
[13] W. Tang, T. Nguyen, R. Howe, Laterally driven poly-silicon resonant microstructures, Sens. Actuators 20 (1989) 25–32.
[14] W. Jones, Roark's Formulas for Stress–Strain, sixth ed., McGraw-Hill, Singapore, 1989, Chapter 7, p. 100.
[15] D. Marcuse, Loss analysis of single-mode fibres splice, Bell. Syst. Technol. J. 56 (1977) 703–718.
[16] S. Nemoto, T. Makimoto, Analysis of splice loss in single-mode fibres using a Gaussian field approximation, Optical Quantum Electron. 11 (1979) 447–457.